A Two-step Fan-beam Backprojection Slice Theorem

Patricio Guerrero and Eduardo Miqueles*

January 21, 2019

Abstract

In this work, we propose a theoretical formulation for the tomographic linear fan-beam backprojection having low computational cost. The proposed formula is obtained from a recent backprojection formulation for the parallel case, with low complexity. We provide a Bessel-Neumann series representation for the backprojection without rebinning of measured data onto a parallel geometry. As a consequence of our representation, there is no loss of resolution on the measured data due to interpolation.

1 Introduction

Fan-beam tomographic measurements are used in different modalities of non-destructive imaging, as those obtained using an x-ray source. A typical tomographic device using a fan-beam geometry is shown in Figure 1. We assume that the distance between the pair source-detector is high if compared to the size of the sample. This is a widely used and known technique, and there are many reconstruction algorithms for this configuration. After being generated with a given aperture angle and a fixed distance source-detector, the wavefront hits the sample originating a signal (or image) on the detector. Different propagation regimes can be considered with a varying distance [10], although we will consider a pure mathematical signal idealized as the Radon transform of the given object. For the parallel tomographic case by means of the classical

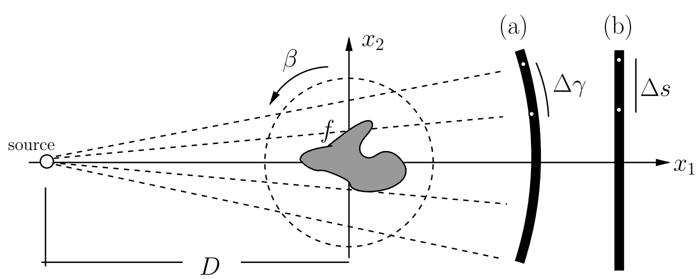

Figure 1: Tomographic setup for a fan-beam geometry: (a) *standard* detector, i.e., equispaced angular mesh with $\Delta\gamma$; sinograms obtained here are denoted by $w(\gamma, \beta)$ (b) *linear* detector, i.e., equispaced regular mesh at the detector with Δs; sinograms obtained here are denoted by $g(s, \beta)$

backprojection formulation for image reconstrution, we can use the recently backprojection slice theorem formulation [12]. It is a formula that reduces a complete backprojection from a computational cost of $O(n^3)$ to $O(n^2 \log n)$ with n the number of pixels in the final reconstructed image. In this work, we want to take advantage of that formulation for two other popular fan-beam geometries, that are a) equispaced angles within the fan with a regular size $\Delta\gamma$, and b) equispaced points in the detector with a mesh Δs. As indicated in [14], we refer to each acquisition as *standard fan* and *linear fan*, respectively, and illustrated at Figure 1.(a) and 1.(b). The linear case is easier to be implemented at a synchrotron beamline, whereas the first is more

*P.Guerrero and E.Miqueles are with the Scientific Computing Group from the Brazilian Synchrotron Light Laboratory at the Brazilian Center for Research in Energy and Materials, Brazil, Campinas-SP. First author is funded by CAPES no. 88887296141201800. E-mail: eduardo.miqueles@lnls.br

used in the medical case . We focus on the the linear detector, as is the reality for a synchrotron beamline. Also, benchtop CT scanners, also based on the conventional cone-beam geometry could take advantage of the approach presented in this work. For completeness, we discuss either the equiangular and the equispaced case.

As indicated in [18, 16], a generalized Fourier slice Theorem for the case of fan-beam geometries is obtained, but presenting the same computational complexity as a conventional backprojection in the parallel case. Also, a rebinning algorithm is performed on the measured data, which is not desirable in our case. Further relations on the frequency domain were obtained in [8] where a rebinning is also necessary. A more elegant approach was established in [2], but a rebinning in the frequency domain is also mandatory. Further advanced rebinning techniques were also stablished in [6] using a hierarchical approach. A series formulation where the backprojection is presented as the first order approximation for a general inversion in the standard fan-beam geometry was presented in [15].

The Radon transform is defined as the linear operator $\mathcal{R}\colon U \to V$ with U being the space of rapidly decreasing functions defined on $\mathbb{R}^2$, so called *feature* space; and V is the *sinogram* space defined on the domain $\mathbb{R} \times [0, \pi]$. For each function $f = f(\boldsymbol{x}) \in U$, $p = \mathcal{R}f$ is defined through

$$p(t, \theta) = \mathcal{R}f(t, \theta) = \int_{\mathbb{R}} f(t\boldsymbol{\xi}_\theta + s\boldsymbol{\xi}_\theta^\perp)\mathrm{d}s$$

with $\boldsymbol{\xi}_\theta = (\cos\theta, \sin\theta)$. The adjoint operator [13] of $\mathcal{R}$, so called *backprojection*, is defined by

$$p \mapsto b(\boldsymbol{x}) = \mathcal{B}p(\boldsymbol{x}) = \int_0^\pi p(\boldsymbol{x} \cdot \boldsymbol{\xi}_\theta, \theta)\mathrm{d}\theta. \tag{1}$$

Computing $\mathcal{B}$ could be extremely expensive for discrete versions of the sinogram p and the backprojected image b, where $\boldsymbol{x}$ covers a domain with a large number of points (pixels in practice) and also (t, θ) covers a large number of pixels and a variety of angles (according to Crowther's criteria [3]). This is the case for synchrotron tomographic projections using high-resolution detectors with more than 2048×2048 pixels and more than 2048 angles. Recently [12], a low-complexity formulation for computing $\mathcal{B}$ was obtained in the frequency domain using polar coordinates, i.e.,

$$\widehat{\mathcal{B}p}(\sigma\boldsymbol{\xi}_\theta) = \frac{\hat{p}(\sigma, \theta)}{\sigma}. \tag{2}$$

The action of $\{\mathcal{R}, \mathcal{B}\}$ is presented in Figure 2. It is a well known fact that $\{p, f\}$ are related through the *Fourier slice Theorem* [13], while $\{b, p\}$ through the *backprojection slice theorem* [12].

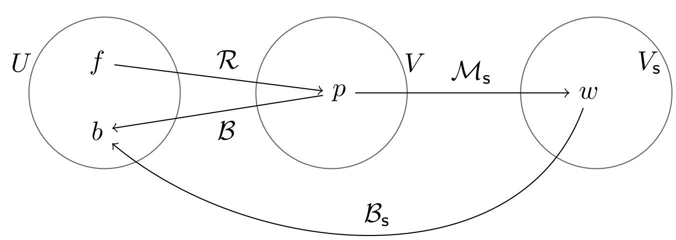

Figure 2: Action diagram for operators $\{\mathcal{B}, \mathcal{R}\}$ and $\{\mathcal{B}_{\mathsf{s}}, \mathcal{R}_{\mathsf{s}}\}$, with $\mathcal{R}_{\mathsf{s}} = \mathcal{M}_{\mathsf{s}}\mathcal{R}$, $\mathcal{B}_{\mathsf{s}} = \mathcal{B}\mathcal{M}_{\mathsf{s}}^*$ and a generalized change of variables $\mathcal{M}_{\mathsf{s}}$.

There exist two different fan-beam geometries for the Radon transform operation [7], the first $\mathcal{R}_{\mathsf{s}}\colon U \to V_{\mathsf{s}}$ is referred as the *standard-fan-sinogram*, where the domain of sinograms lies within the interval $[-\frac{\pi}{2}, \frac{\pi}{2}] \times [0, 2\pi]$. The second case, $\mathcal{R}_\ell\colon U \to V_\ell$ is referred as the *linear-fan-sinogram*, with sinograms having the domain varying within the interval $\mathbb{R} \times [0, 2\pi]$. Acting on the feature function f, $\mathcal{R}_{\mathsf{s}}$ and $\mathcal{R}_\ell$ are defined respectively, as

$$w(\gamma, \beta) = \mathcal{R}f(D\sin\gamma, \beta + \gamma), \tag{3}$$

and

$$g(s,\beta) = \mathcal{R}f(\frac{sD}{\sqrt{s^2+D^2}}, \beta + \arctan\frac{s}{D}), \tag{4}$$

Since both operations represent a change of variables in the classical parallel sinogram, we can use the following notation,

$$\mathcal{R}_{\mathsf{s}} f(\gamma,\beta) = \mathcal{M}_{\mathsf{s}}\mathcal{R}f(\gamma,\beta), \quad \mathcal{R}_{\ell} f(s,\beta) = \mathcal{M}_{\ell}\mathcal{R}f(s,\beta) \tag{5}$$

with $\mathcal{M}_{\mathsf{s}}$ and $\mathcal{M}_\ell$ acting on a parallel sinogram p, respectively as

$$\begin{aligned} \mathcal{M}_{\mathsf{s}} p(\gamma,\beta) &= p(D\sin\gamma, \gamma+\beta), \\ \mathcal{M}_\ell p(s,\beta) &= p(\frac{sD}{\sqrt{s^2+D^2}}, \beta + \arctan\frac{s}{D}). \end{aligned} \tag{6}$$

It is clear that for the change of variables operation $\mathcal{M}_{\mathsf{s}}$, the situation is depicted in Figure 2. From the experimental point of view, we assume that the origin is centered in the object, with D being the distance of the focal point source to the origin. The angle γ indicates a point within the solid angle that completely covers the detector whereas s is the distance on the detector with respect to the rotation axis, as indicated by Figure 1. Since is true that $\mathcal{R}_{\mathsf{s}} = \mathcal{M}_{\mathsf{s}}\mathcal{R}$, a conventional functional relation for space U and V_{s} provide us with the following statement,

$$\langle \mathcal{R}_{\mathsf{s}} f, g\rangle_{V_{\mathsf{s}}} = \langle \mathcal{M}_{\mathsf{s}}\mathcal{R}f, g\rangle_{V_{\mathsf{s}}} \tag{7}$$

$$= \langle \mathcal{R}f, \mathcal{M}_{\mathsf{s}}^* g\rangle_V = \langle f, \mathcal{R}^*\mathcal{M}_{\mathsf{s}}^* g\rangle_U \tag{8}$$

with $\cdot^*$ standing for the adjoint operation and $\langle\cdot,\cdot\rangle_{V_{\mathsf{s}}}$, $\langle\cdot,\cdot\rangle_V$, $\langle\cdot,\cdot\rangle_U$ standard L^2 inner products. Also, $\mathcal{M}_{\mathsf{s}}^*$ stands for the adjoint operator of $\mathcal{M}_{\mathsf{s}}$. Now, since $\mathcal{R}^* = \mathcal{B}$, it follows that $\mathcal{R}_{\mathsf{s}}^* = \mathcal{B}\mathcal{M}_{\mathsf{s}}^*$. In this work we propose a Fourier approach for the equation $\mathcal{R}_\ell^* = \mathcal{B}\mathcal{M}_\ell^*$ using several properties from operation $\mathcal{M}_{\mathsf{s}}$.

1.1 Conventional fan-beam backprojectors

The adjoint operator for fan-beam Radon transforms is a weighted backprojection operator of the standard parallel one [7]. Considering the geometry indicated at Figure 1, we provide two main results for the adjoint transform of operators $\mathcal{R}_{\mathsf{s}}$ and $\mathcal{R}_\ell$. For completeness, we denote $\boldsymbol{r}_\beta = D\boldsymbol{\xi}_\beta^\perp$.

Lemma 1. The operator $g \in V_\ell \mapsto \mathcal{B}_\ell g \in U$ defined by

$$\mathcal{B}_\ell g(\boldsymbol{x}) = \int_0^{2\pi} \frac{1}{D\ U_\beta(\boldsymbol{x})} \sqrt{s_\beta^2 + D^2}\, g(s_\beta,\beta)\,\mathrm{d}\beta, \tag{9}$$

is the adjoint of $\mathcal{R}_\ell$ in the sense of (8). Taking $\boldsymbol{x} = r\boldsymbol{\xi}_\phi$, $U_\beta(\boldsymbol{x}) = (D + r\sin(\beta-\phi))/D$ and s_β as the corresponding s-value for $\boldsymbol{x}$ at a source angle β, i.e., $s_\beta = Dr\sin(\beta-\phi)/(D+r\sin(\beta-\phi))$.

Proof. A simple change of variables; see [7, 4]. □

Lemma 2. The operator $w \in V_{\mathsf{s}} \mapsto \mathcal{B}_{\mathsf{s}} w \in U$ defined by

$$\mathcal{B}_{\mathsf{s}} w(\boldsymbol{x}) = \int_0^{2\pi} \frac{1}{L_\beta(\boldsymbol{x})}\, w(\gamma_\beta,\beta)\,\mathrm{d}\beta, \tag{10}$$

is the the adjoint of $\mathcal{R}_{\mathsf{s}}$, in the sense of (8). Here, $L_\beta = \|\boldsymbol{r}_\beta - \boldsymbol{x}\|_2$ is the distance of source with the backprojected position $\boldsymbol{x}$ and γ_β is the angle of such point within the fan, i.e., $\cos\gamma_\beta = \boldsymbol{r}_\beta\cdot(\boldsymbol{r}_\beta - \boldsymbol{x})$.

Proof. A simple change of variables; see [7, 4]. □

1.2 Two-step backprojection formulas

As discussed in (8), the adjoint of $\{\mathcal{M}_\mathsf{s}, \mathcal{M}_\ell\}$ plays an important role for our final adjoint formulation. The adjoint operator of $\mathcal{M}_\ell$ is defined for $g \in V_\ell$ by

$$\mathcal{M}_\ell^* g(t,\theta) = g(\underbrace{\frac{tD}{\sqrt{D^2-t^2}}}_{\ell(t)}, \underbrace{\theta - \arcsin\frac{t}{D}}_{\kappa(t,\theta)}) \underbrace{\frac{D^3}{(D^2-t^2)^{3/2}}}_{h(t)}, \tag{11}$$

for D larger to the radius of the circumference containing the sample. To verify that this is true, we select an arbitrary fan-beam sinogram $p \in V_\ell$, proving that $\langle \mathcal{M}_\ell p, g\rangle_{V_\ell} = \langle p, \mathcal{M}_\ell^* g f\rangle_V$. This is a trivial exercise from change of variables. In fact, starting with the definition of $\mathcal{M}_\ell$ we obtain

$$\begin{aligned}\langle \mathcal{M}_\ell p, g\rangle_{V_\ell} &= \int_{[0,2\pi]\times\mathbb{R}} \mathcal{M}_\ell p(s,\beta) g(s,\beta)\,\mathrm{d}s\mathrm{d}\beta \\ &= \int_{[0,\pi]\times\mathbb{R}} p(t,\theta) g(\frac{tD}{\sqrt{D^2-t^2}}, \theta - \arcsin\frac{t}{D}) \frac{D^3}{(D^2-t^2)^{3/2}} \mathrm{d}t\mathrm{d}\theta.\end{aligned}$$

from where (11) is obtained. It is also straightforward to prove that, for $w \in V_\mathsf{s}$, the adjoint operator of $\mathcal{M}_\mathsf{s}$ is defined by

$$\mathcal{M}_\mathsf{s}^* w(t,\theta) = w(\underbrace{\arcsin\frac{t}{D}}_{\gamma(t)}, \theta - \arcsin\frac{t}{D}) \underbrace{\frac{1}{\sqrt{D^2-t^2}}}_{h(t)}, \tag{12}$$

It is clear that both operators $\mathcal{M}_\mathsf{s}, \mathcal{M}_\ell$ satisfies the property

$$\mathcal{M}_\ell^* = h(t)\mathcal{M}_\ell^{-1}, \quad \text{or} \quad \mathcal{M}_\mathsf{s}^* = h(t)\mathcal{M}_\mathsf{s}^{-1}. \tag{13}$$

We are not differentiating function h, as is clear from the context of symbols, either $\mathcal{M}_\mathsf{s}$ or $\mathcal{M}_\ell$. The formal adjoints of $\mathcal{R}_\mathsf{s}$ and $\mathcal{R}_\ell$ are presented in Lemmas 1 and 2. The problem with these formulations is the difficulty for a low-cost implementation algorithm. To circumvent this problem, we use the fact that $\{\mathcal{R}, \mathcal{B}\}$ are bounded operators between Hilbert spaces U and V - here understood as the space of rapidly decreasing functions with two-variables. Hence, we obtain the following result.

Theorem 1. *Considering fan-beam geometries, a formal adjoint for each operator $\mathcal{R}_\mathsf{s}$ and $\mathcal{R}_\ell$ is given explicitly by equations (10) and (9), which on the other hand, are also given exactly by $\mathcal{B}_\ell^* = \mathcal{B}\mathcal{M}_\ell^*$ and $\mathcal{B}_\mathsf{s}^* = \mathcal{B}\mathcal{M}_\mathsf{s}^*$ respectively.*

Proof. This is an immediate consequence of the uniqueness of the adjoint for bounded operators on Hilbert spaces. In fact, since $\mathcal{B}$ and $\mathcal{M}_\ell^*$ are bounded, the composition will also be bounded, the same applies for $\mathcal{M}_\mathsf{s}^*$. □

2 Main result

As is easy to note using an appropriate change of variables, given a sinogram $g(s,\beta) \in V_\ell$, the Fourier transform of $\mathcal{M}_\ell^* g(t,\theta)$ with respect to t is given by

$$\begin{aligned}\widehat{\mathcal{M}_\ell^* g}(\sigma,\theta) &= \int_\mathbb{R} h(t) g(\ell(t), \kappa(t,\theta)) e^{-it\sigma}\mathrm{d}t \\ &= \int_\mathbb{R} g\left(v, \theta - \arcsin\frac{v}{D}\right) e^{-i\frac{vD\sigma}{\sqrt{D^2+v^2}}}\mathrm{d}v\end{aligned} \tag{14}$$

Analogously, taking $w(\gamma,\beta) \in V_\mathsf{s}$, the Fourier transform of $\mathcal{M}_\mathsf{s}^* w(t,\theta)$ with respect to t is

$$\begin{aligned}\widehat{\mathcal{M}_\mathsf{s}^* w}(\sigma,\theta) &= \int_\mathbb{R} h(t) w(\gamma(t), \theta - \gamma(t)) e^{-it\sigma}\mathrm{d}t \\ &= \int_0^{2\pi} w\left(v, \theta - v\right) e^{-iD\sigma\sin v}\mathrm{d}v\end{aligned} \tag{15}$$

From (14) and (15) we note that, for a fixed θ, it is difficult to compute numerically the sinogram $g(v, \theta - \arcsin\frac{v}{D}) \in V_\ell$ due to the nonlinear effect provided by the inverse trigonometric function. On the other hand, it is easier to compute the sinogram $Z(v,\theta) = w(v, \theta - v) \in V_{\mathsf{s}}$ due to the linear factor $\theta - v$ without a significance loss on the sinogram angular resolution.

Let us consider the case $w \in V_{\mathsf{s}}$, where sinogram $Z(v,\theta) = w(v,\theta - v)$ is 2π-periodic function with respect to v. After expanding it on a Fourier series, (15) becomes

$$\widehat{\mathcal{M}_{\mathsf{s}}^* g}(\sigma,\theta) = \sum_n c_n(\theta; w) \int_0^{2\pi} e^{i[nv - D\sigma \sin v]} \mathrm{d}v \tag{16}$$

$$= 2\pi \sum_n c_n(\theta; w) J_n(D\sigma) \tag{17}$$

with

$$c_n(\theta; w) = \frac{1}{2\pi}\int_0^{2\pi} Z(v,\theta) e^{-inv} \mathrm{d}v \tag{18}$$

and $\{J_n\}$ a sequence of Bessel functions of first kind $\{J_n\}$. This same result can not be obtained for the operation $\widehat{\mathcal{M}_\ell^* g}(\sigma,\theta)$ because of the noniteroperability of exponent $vD\sigma/\sqrt{D^2+v^2}$ with Bessel functions. Using the property $J_{-n}(x) = (-1)^n J_n(x)$ we finally obtain the Bessel-Neumann series

$$\widehat{\mathcal{M}_{\mathsf{s}}^* w}(\sigma,\theta) = \sum_{n=0}^{\infty} b_n(\theta; Z) J_n(D\sigma) \tag{19}$$

with $b_0 = c_0$ and $b_n = [c_n + (-1)^n \bar{c_n}]$ for $n \geq 1$.

Switching between fan-beam geometries requires only a one-dimensional interpolation on the first variable. In fact, taking $g \in V_\ell$, the operation $\mathcal{L}$ defined by

$$w(\gamma,\beta) = \mathcal{L}g(\gamma,\beta) = g(D\tan\gamma, \beta) \iff \mathcal{R}_{\mathsf{s}} = \mathcal{L}\mathcal{R}_\ell \tag{20}$$

provide a sinogram w lying at space V_{s}. Such an operator has an inverse given by $\mathcal{L}^{-1}h(s,\beta) = h(\arctan\frac{s}{D}, \beta)$ in such a way that the adjoint operation is

$$\mathcal{L}^* h(s,\beta) = a(s)\mathcal{L}^{-1}h(s,\beta), \quad a(s) = \frac{D}{D^2+s^2} \tag{21}$$

The following Theorem is the main result enabling us to provide a two-step backprojection algorithm for the fan-beam *linear* geometry.

Theorem 2. *The backprojections $\mathcal{B}_{\mathsf{s}}$ and $\mathcal{B}_\ell$ are related through $\mathcal{B}_\ell g = \mathcal{B}_{\mathsf{s}}\tau\mathcal{L}g$, with $\tau(\gamma) = D\sec^2\gamma$, for all $g \in V_\ell$.*

Proof. Starting with $\mathcal{B}_{\mathsf{s}} = \mathcal{R}_{\mathsf{s}}^*$ and using (20) we obtain

$$\mathcal{B}_{\mathsf{s}} = (\mathcal{L}\mathcal{R}_\ell)^* = \mathcal{R}_\ell^*\mathcal{L}^* = \mathcal{B}_\ell\mathcal{L}^*$$

from where follows $\mathcal{B}_\ell = \mathcal{B}_{\mathsf{s}}(\mathcal{L}^*)^{-1}$. Using (21) and the fact that $(\mathcal{L}^*)^{-1} = a(s(\gamma))^{-1}\mathcal{L}$ with $s(\gamma) = D\tan\gamma$, the proposed equation is obtained. □

Now, using the fact that $\mathcal{B}_{\mathsf{s}}$ and $\mathcal{B}$ are related (from Theorem 1), our resulting formulation for the linear fan-beam backprojection is obtained by the following construction:

(i) Let $g \in V_\ell$ be an linear fan-beam sinogram (as depicted in Fig.1) and let $z(\gamma,\beta) = \tau(\gamma)w(\gamma,\beta)$ with $w = \mathcal{L}g$ be his representation at space V_{s}. From z we compute $Z = \mathcal{A}z$ defined as $Z(\gamma,\theta) = z(\gamma, \theta - \gamma)$

(ii) Since $\mathcal{B}_{\mathsf{s}} = \mathcal{B}\mathcal{M}_{\mathsf{s}}^*$, it follows that the Fourier transform of $\mathcal{B}_{\mathsf{s}}$ at the polar frequency $\sigma\boldsymbol{\xi}_\theta$ is

$$\widehat{\mathcal{B}_\ell g}(\sigma\boldsymbol{\xi}_\theta) \overset{\text{Theo.1}}{=} \widehat{\mathcal{B}_{\mathsf{s}}(\mathcal{L}^*)^{-1}g}(\sigma\boldsymbol{\xi}_\theta) \tag{22}$$

$$\overset{\text{(i)}}{=} \widehat{\mathcal{B}_{\mathsf{s}}\tau\mathcal{L}g}(\sigma\boldsymbol{\xi}_\theta) = \widehat{\mathcal{B}_{\mathsf{s}}z}(\sigma\boldsymbol{\xi}_\theta) \tag{23}$$

$$\overset{\text{Theo.2}}{=} \widehat{\mathcal{B}\mathcal{M}_{\mathsf{s}}^* q}(\sigma\boldsymbol{\xi}_\theta) \tag{24}$$

$$\overset{\text{BST}}{=} \frac{\widehat{\mathcal{M}_{\mathsf{s}}^* q}(\sigma\boldsymbol{\xi}_\theta)}{\sigma} \tag{25}$$

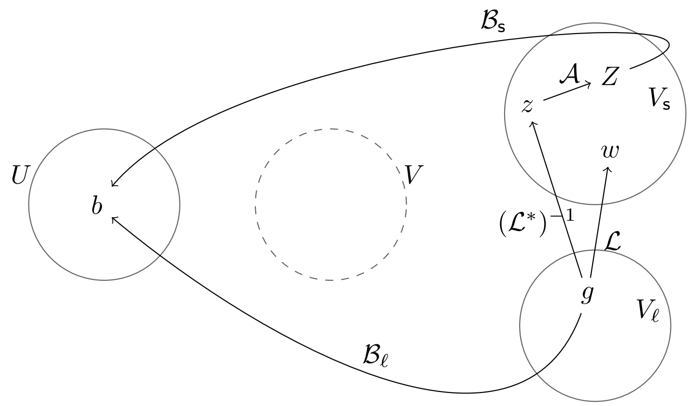

Figure 3: diagram for the backprojection operator $\mathcal{B}_\ell$ (without rebinning to space V) through the action of $(\mathcal{L}^*)^{-1}$, $\mathcal{A}$ and $\mathcal{B}_\mathsf{s}$. Here, $z = \tau\ w$,with τ as described in Theorem 2. See text for details.

(iii) From (19) the backprojection finally becomes as the following Bessel Neumann series

$$\widehat{\mathcal{B}_\ell g}(\sigma \boldsymbol{\xi}_\theta) = \underbrace{\frac{1}{\sigma}\sum_{n=0}^{\infty} b_n(\theta; Z) J_n(D\sigma)}_{\mathcal{N}g(\sigma,\theta)}, \tag{26}$$

with $Z = \mathcal{A}z$ and $(\sigma, \theta) \in \mathbb{R}_+ \times (0, 2\pi]$.

Figure 3 illustrate the action of our method, where a backprojection $b \in U$ is obtained in two-steps. The unknown backprojection $\mathcal{B}_\ell g$ is obtained in the frequency domain from (26), using polar coordinates through two main operations to obtain sinogram $Z \in V_\mathsf{s}$ through $\mathcal{L}$ (interpolation on the first variable) and $\mathcal{A}$ (interpolating at the second variable). It is important to note that $\{b_n\}$ are easily (and rapidly) computed from Z using the Fast Fourier transform. Also, the sequence $\{J_n\}$ can be used as a *lookup table* for the computation of (26), not being costly at computing time. For $g \in V_\ell$, the support of an impulse response of the sequence $\{w = \mathcal{L}g, z = \tau w, Z = \mathcal{A}z\}$ is presented in Figure 4.

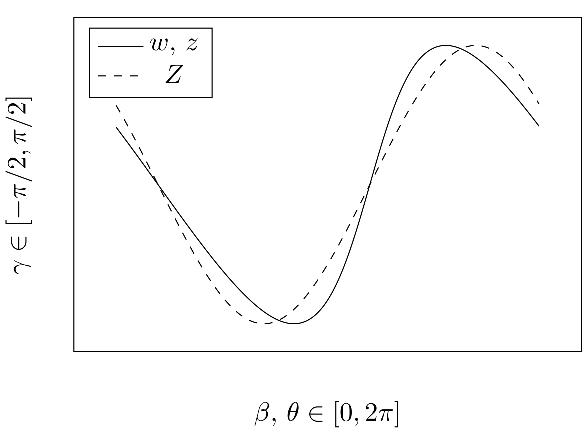

Figure 4: Support of an impulse response for both $w = \mathcal{L}g$, $z = \tau w$ (solid) and for $Z = \mathcal{A}z$ in (dashed). Note that Q takes a parallel sinogram support due to the act of $\mathcal{A}$.

3 An implicit Fourier slice approach

Considering the diagram of Figure 2, and given a linear fan-beam data $g \in V_\ell$, the standard algorithmic approach for inversion of g requires a rebinning of g to the parallel geometry space V, followed by any Fourier strategy for numerical inversion, e.g., gridding [11], filtered backprojection [4] or other analytical approach.

Considering the following regularized least squares problem

$$\underset{f \in U}{\text{minimize}} \, \|\mathcal{R}_\ell f - g\|_{V_\ell}^2 + \lambda \|f\|_U^2 \tag{27}$$

and the Euler-Lagrange equations for the optimality condition, we known that f minimizes (27) if and only if (see [9, 12]) the following normal equations are equivalent: $[\mathcal{R}_\ell^* \mathcal{R}_\ell + \lambda \mathcal{I}] f(\boldsymbol{x}) = \mathcal{R}_\ell^* g(\boldsymbol{x}) \iff [\mathcal{B}_\ell \mathcal{R}_\ell + \lambda \mathcal{I}] f(\boldsymbol{x}) = \mathcal{B}_\ell g(\boldsymbol{x}) \iff [\mathcal{B} \mathcal{M}_\ell^* \mathcal{M}_\ell \mathcal{R} + \lambda \mathcal{I}] f(\boldsymbol{x}) = \mathcal{B}_\ell g(\boldsymbol{x})$. Since $\mathcal{M}_\ell^* \mathcal{M}_\ell = h\mathcal{I}$ the normal equations becomes

$$\mathcal{B}(h\mathcal{R}f) + \lambda f = \mathcal{B}_\ell g \tag{28}$$

Finally, applying the Fourier transformation on (28), changing to polar coordinates and using the BST formulation [12], we obtain the following result

$$\frac{\widehat{h\mathcal{R}f}(\sigma, \theta)}{\sigma} + \lambda \hat{f}(\sigma \boldsymbol{\xi}_\theta) = \widehat{\mathcal{B}_\ell g}(\sigma \boldsymbol{\xi}_\theta) \tag{29}$$

According to (26) and the classical Fourier slice Theorem, the above equation is also equivalent to

$$\widehat{h}(\sigma) \star \hat{f}(\sigma \boldsymbol{\xi}_\theta) + \sigma \lambda \hat{f}(\sigma \boldsymbol{\xi}_\theta) = \mathcal{N} g(\sigma, \theta), \tag{30}$$

which can be interpreted as regularized and implicit version for the Fourier-Slice-Theorem and can be used to obtain f iteratively in the frequency domain. Here, we emphasize that $\mathcal{N}g$ does not contain a strong rebinning, as typically required by algorithms pointed out in the literature, and each Bessel function defining the operator $\mathcal{N}$ can be computed only once.

4 Conclusions

We have proposed in this work a two-step backprojection algorithm for fan-beam scanning with linear detectors. The first step consists on a sequence of simple one-dimensional operators where a fan-beam *standard* sinogram is obtained. The second step, the backprojection operation, is performed by writing the Fourier transform of the backprojected image as a Bessel-Neumann series on the frequency variable σ weighted by $1/\sigma$. The coefficients of the expansion are in fact the Fourier coefficients of the sinogram obtained in the first step. This approach, based on the low cost backprojection BST formula [12] for parallel sinograms, presents the same reduction on the computational cost related to conventional fan-beam backprojections. A second interesting feature is the absence of a rebinning process from fan to parallel beam projections as is mostly done in other fan-backprojection algorithms. When dealing with standard fan-beam data, the first step is more straightforward where only one linear change of variables is needed than can be performed through a $\pi/4$ rotation of the sinogram without lying on interpolations.

Once the backprojection for linear fan sinograms is efficiently performed, a complete inversion algorithm can be implemented for cone-beam tomography with plane detectors. The FDK formula [5] is widely used for this aim. Briefly, the cones are considered as a set sloped fans having the same source in $\mathbb{R}^3$ and parallel line detectors placed over the plane detector. A change of variables [17] is needed to write a fan in $\mathbb{R}^2$ as a sloped fan in $\mathbb{R}^3$ and backproject it. The convoution filter is easily derived similar to the parallel beam case. Details of the full reconstruction using the FDK formula are presented in [14].

Finally, the Bessel-Neumann representation for the Backprojection $\mathcal{B}_\ell g$ in the frequency domain (26) can be computed numerically with a limited number of terms N. This is true due to the fact that $J_n(x)/x$ has a pointwise convergence to zero due to $|J_n(x)| \leq |\frac{1}{2}x|^n/n!$ for all $x \in \mathbb{R}_+$ [1, eq. 9.1.62]. Finding the right choice for N is a study beyond the scope of this work.

References

[1] Milton Abramowitz and Irene A. Stegun, editors. *Handbook of Mathematical Functions with Formulas, Graphs, and Mathematical Tables.* National Bureau of Standards, 1964.

[2] Guang-Hong Chen, Shuai Leng, and Charles A Mistretta. A novel extension of the parallel-beam projection-slice theorem to divergent fan-beam and cone-beam projections. *Medical physics*, 32(3):654–665, 2005.

[3] Richard Anthony Crowther, DJ DeRosier, and Aaron Klug. The reconstruction of a three-dimensional structure from projections and its application to electron microscopy. *Proc. R. Soc. Lond. A*, 317(1530):319–340, 1970.

[4] Stanley R Deans. *The Radon transform and some of its applications.* Courier Corporation, 2007.

[5] L. A. Feldkamp, L. C. Davis, and J. W. Kress. Practical cone-beam algorithm. *J. Opt. Soc. Am. A*, 1(6):612–619, Jun 1984.

[6] AK George and Y Bresler. A fast fan-beam backprojection algorithm based on efficient sampling. *Physics in Medicine & Biology*, 58(5):1415, 2013.

[7] Avinash C. Kak and Malcolm Slaney. *Principles of computerized tomographic imaging.* Society for Industrial and Applied Mathematics, 2001.

[8] Daniil Kazantsev and Valery Pickalov. Fan-beam tomography iterative algorithm based on fourier transform. In *Nuclear Science Symposium Conference Record, 2008. NSS'08. IEEE*, pages 4138–4139. IEEE, 2008.

[9] David G Luenberger. *Optimization by vector space methods.* John Wiley & Sons, 1997.

[10] D Russell Luke, James V Burke, and Richard G Lyon. Optical wavefront reconstruction: Theory and numerical methods. *SIAM review*, 44(2):169–224, 2002.

[11] F Marone and M Stampanoni. Regridding reconstruction algorithm for real-time tomographic imaging. *Journal of synchrotron radiation*, 19(6):1029–1037, 2012.

[12] Eduardo Miqueles, Nikolay Koshev, and Elias S Helou. A backprojection slice theorem for tomographic reconstruction. *IEEE Transactions on Image Processing*, 27(2):894–906, 2018.

[13] Frank Natterer. *The mathematics of computerized tomography*, volume 32. Siam, 1986.

[14] Frank Natterer and Frank Wübbeling. *Mathematical methods in image reconstruction*, volume 5. Siam, 2001.

[15] Yuchuan Wei, Ge Wang, and Jiang Hsieh. Relation between the filtered backprojection algorithm and the backprojection algorithm in ct. *IEEE Signal Processing Letters*, 12(9):633–636, 2005.

[16] S-R Zhao and H Halling. A new fourier method for fan beam reconstruction. In *Nuclear Science Symposium and Medical Imaging Conference Record, 1995., 1995 IEEE*, volume 2, pages 1287–1291. IEEE, 1995.

[17] Shuang-Ren Zhao, Dazong Jiang, Kevin Yang, and Kang Yang. Generalized fourier slice theorem for cone-beam image reconstruction. *Journal of X-ray science and technology*, 23(2):157–188, 2015.

[18] Shuangren Zhao, Kang Yang, and Kevin Yang. Fan beam image reconstruction with generalized fourier slice theorem. *Journal of X-ray Science and Technology*, 22(4):415–436, 2014.